Available online at www.sciencedirect.com

ScienceDirect

Ceramics International 39 (2013) 9253–9261

CERAMICS INTERNATIONAL

www.elsevier.com/locate/ceramint

MCr_2O_4 (M = Co, Cu, and Zn) nanospinels for 2-propanol combustion: Correlation of structural properties with catalytic performance and stability

S.A. Hosseini[a,*], M.C. Alvarez-Galvan[b], J.L.G. Fierro[b], A. Niaei[c], D. Salari[c]

[a]Department of Chemistry, Faculty of Science, Urmia University, 57159 Urmia, Iran
[b]Instituto de Catálisis y Petroleoquímica, CSIC, Cantoblanco, E-28049 Madrid, Spain
[c]Department of Applied Chemistry, University of Tabriz, Tabriz, Iran

Received 21 April 2013; accepted 9 May 2013
Available online 30 May 2013

Abstract

The correlation between structure and activity of MCr_2O_4 nanospinels (M = Co, Cu, and Zn) synthesized by a sol–gel combustion method was investigated for the oxidation of 2-propanol. The catalysts were characterized by Fourier transform infrared spectroscopy (FTIR), X-ray diffraction (XRD), N_2 adsorption/desorption, temperature programmed reduction (TPR), X-ray photoelectron spectroscopy (XPS), and scanning electron microscopy (SEM). Wide-angle XRD patterns show that the samples are pure spinel phases with cubic structure for $CoCr_2O_4$ and $ZnCr_2O_4$, and tetragonal structure for $CuCr_2O_4$. FTIR spectra confirmed the spinel structure of samples. The spinels were tested for total oxidation of 2-propanol as a model reaction for the catalytic combustion of oxygenated organic pollutants. $ZnCr_2O_4$ exhibited the highest activity and stability than the others toward the combustion of 2-propanol. The higher activity of $ZnCr_2O_4$ was ascribed to existence of excess surface oxygen on catalyst, active Cr^{3+}–Cr^{6+} pair sites, and synergistic effect between ZnO and $ZnCr_2O_4$ confirmed by TPR and XPS techniques. The high stability of $ZnCr_2O_4$ and $CuCr_2O_4$ was explained by the existence of stable Cr^{6+} species on the surface of catalysts. The study showed that $ZnCr_2O_4$ could be used as a promising catalyst in the catalytic conversion of organic compounds.

Keywords: D. Spinel; Nanooxide; Catalysis; VOC; XPS

1. Introduction

Total catalytic oxidation technology is widely used in several industrial processes for air pollution abatement. Compared with thermal combustion techniques, higher efficiencies at lower operating temperatures are reached, obtaining considerable environmental and economic benefits [1–3]. Driven by the need of decreasing manufacturing cost and increasing resistance to poisoning of commercial catalysts for volatile organic compounds (VOCs) elimination, efforts have been made to develop metal oxide catalysts, which can exhibit activity similar or higher than noble metal catalysts [4]. Among mixed oxides, spinel and perovskite-type oxides are promising in various fields due to their high thermal resistance and electronic properties. They are used in sensor and semiconductor technology as well as in heterogeneous catalysis [5,6].

Cobalt, copper, zinc and chromium oxides are the most frequently used oxides to reduce air pollution by total oxidation of hydrocarbons [7,8]. Improved properties of mixed oxides against individual oxides are well known, especially in the environmental catalysis. In particular, $CuCo_2O_4$ and $CoCr_2O_4$ spinels were found to be very active for hydrocarbons oxidation and removal of air pollutants [9–13].

Yan et al. reported the excellent catalytic performance of $Zn_xCo_{1-x}Co_2O_4$ spinel catalysts for the decomposition of nitrous oxide and concluded that the partial replacement of Co^{2+} by Zn^{2+} in Co_3O_4 spinel oxide led to a significant improvement in the catalytic activity for the N_2O decomposition, being the catalytic activity dependent on the degree of Co^{2+} substitution by Zn^{2+} [14]. Among the transition metal oxides, chromium oxide has been known to be the most active phase [1,15]. Chromite spinels are, moreover, thermally stable

*Corresponding author. Tel.: +98 441 2972166.
E-mail address: a.hosseini@urmia.ac.ir (S.A. Hosseini).

0272-8842/$ - see front matter © 2013 Elsevier Ltd and Techna Group S.r.l. All rights reserved.
http://dx.doi.org/10.1016/j.ceramint.2013.05.033

and maintain enhanced and sustained activities for a variety of reactions [16].

High surface areas of solid particles are of predominant importance for processes taking place at the phase boundary between solid particles and a liquid or gas phase. Thus, spinels with high surface areas are interesting for catalytic processes, the preparation method being essential to get a good performance of these mixed oxides [13,17,18]. Among different methods used for the synthesis of metal oxides, the sol–gel method has a promising potential [19] due to the relatively low calcination temperature required, the high purity and good chemical homogeneity in the final materials. Historically, the sol–gel method has employed the metal alkoxide precursors that readily undergo catalyzed hydrolysis and condensation to form a sol of metal oxide particles of nanoscale dimensions [20].

Inline with the above, this work was undertaken with the aim to study the influence of the nature of cation M (Cu, Co, and Zn) in different chromite spinels (MCr_2O_4) over the structure and performance (activity and stability) in the catalytic oxidation of oxygenated volatile organic compounds (O-VOCs). The synthesis of chromite nanospinels i.e. $CuCr_2O_4$, $CoCr_2O_4$ and $ZnCr_2O_4$ will be carried out by the sol–gel combustion in order to obtain high surface area. 2-Propanol was selected as model of oxygenated organic compounds, because it is commonly used as a solvent in chemical and petrochemical industries [21]. Physical–chemical properties (structure, texture, morphology, surface composition, and redox properties) of catalysts were determined by XRD, BET, SEM, FTIR, XPS and TPR.

2. Materials and methods

2.1. Catalyst preparation

The sol–gel combustion method, described in detail in our previous studies [22,23] was used for the synthesis of the catalysts. Briefly, nitrates of different cations were used as precursors ($Cu(NO_3)_2 \cdot 3H_2O$ (99.5%), $Cr(NO_3)_3 \cdot 9H_2O$ (98%), $Co(NO_3)_2 \cdot 6H_2O$ (99%), $Zn(NO_3)_2 \cdot 6H_2O$ ($>98\%$)), with the stoichiometric ratio M:Cr=1:2 and citric acid monohydrate ($C_6H_8O_7 \cdot H_2O$ (99.5%)) as fuel ([citric acid]/[total nitrates]=0.4). All the chemicals were supplied by Merck. Then, the solution was heated at 80 °C and stirred constantly, which transforms it into a gel. Slow heating of the gel up to 180 °C resulted in an auto-combustion process with the formation of a black fluffy material. The reaction is noticeably exothermic, which leads to a thermal peak in the reacting solid mixture above 1000 °C for a few seconds. The sample was then calcined at 700 °C for 6 h to ensure the absence of carbonaceous residues which may remain in the samples and the formation of the mixed-oxide phase.

2.2. Catalyst characterization

X-ray diffraction (XRD) measurements were carried out on a SIEMENS D5000 X-ray powder diffractometer equipped with a Kristalloflex 760 X-ray generator provided with a curved graphite monochromator and Cu Kα radiation source (40 kV and 30 mA). The integration time was 3 s per step. Specific BET surface area and pore volume of samples were determined from N_2 isotherms measured at −196 °C using a micropore ASAP 2010 analyzer. SEM characterization was carried out with a scanning electron microscope (model EQ-C1-1). Infrared (IR) spectra were recorded with a Bruker 27 FT-IR spectrometer using the Universal ATR Accessory in the range from 3650 to 400 cm^{-1} with 4 cm^{-1} resolution.

Measurement of the reducibility of different oxides (TPR) was carried out with Micromeritics Autochem 2910 Analyzer. Catalyst samples were pre-treated in air at 500 °C for 1 h in order to clean the catalyst surface before reduction. Hydrogen consumption was measured with a flow of a mixture of 10 vol% H_2 in argon with a flow rate of 50 cm^3 min^{-1} and a linear heating rate of 10 °C/min, 50–900 °C.

XP spectra were obtained with a VG Escalab 200R spectrometer equipped with a hemispherical electron analyzer (constant pass energy of 50 eV) and a Mg Kα ($h\nu$=1254.6 eV) X-ray source, powered at 120 W. The XPS data signals were taken in increments of 0.1 eV with dwell times of 50 ms. Binding energies were calibrated relative to the C 1s peak at 284.8 eV. High resolution spectra envelopes were obtained by curve fitting synthetic peak components using the software *XPS peak*. The raw data were used with no preliminary smoothing. Symmetric Gaussian–Lorentzian product functions were used to approximate the line shapes of the fitting components.

2.3. Evaluation of catalytic performance

Catalytic studies were carried out at atmospheric pressure and different temperatures in a fixed-bed reactor placed in a PID controlled electrical furnace. A loading of 0.20 g of catalyst in powder form was placed into a tubular glass reactor, with length of 40 cm and internal diameter of 8 mm. Packing of the catalyst was accomplished with mechanical vibration, and the two ends of the catalytic bed were plugged with glass wool. The temperature was controlled with a thermocouple placed inside the catalyst bed. Before starting each run, catalysts were pre-treated with 10 mL/min of pure nitrogen at 400 °C in order to eliminate the possible compounds adsorbed on the catalyst surface. After this pretreatment, the reactor was cooled to 100 °C, and the reaction vapor was introduced by passing the carrier gas (nitrogen) flow through a saturator containing the liquid organic compound (2-propanol) and a different air flow was used to maintain the molar concentration of organic compound which is around 0.2% in the full stream. Gas flow is controlled by needle valve (Parker Co.). Flow rates were measured using a soap bubble flow meter. The inlet and outlet concentrations of 2-propanol were carried out in a Shimadzu 2010 gas chromatograph. All experimental runs were taken under steady state conditions.

3. Results and discussion

3.1. Characterization of catalysts

Following the synthesis procedure given in the experimental section, MCr_2O_4 (M=Cu, Co, and Zn) spinels were obtained. Fig. 1 shows XRD patterns of the chromite samples. The characteristic peaks of $ZnCr_2O_4$ (JCPDS 22-1107), $CoCr_2O_4$ (JCPDS 35-1321) and $CuCr_2O_4$ (JCPDS 34-0424) are distinguished in the synthesized samples. $CuCr_2O_4$ showed tetragonal structure; its average crystallite size, as estimated by the Scherrer equation, was 40 nm. On the other hand, $CoCr_2O_4$ and $ZnCr_2O_4$ crystallized in the cubic system with crystal sizes around 40 and 37 nm, respectively. All the samples were single phase and present a spinel structure without other distinguishable peaks attributable to other phases. Table 1 presents the space groups and lattice parameters of samples. These findings are in agreement with the literature reports [24–27].

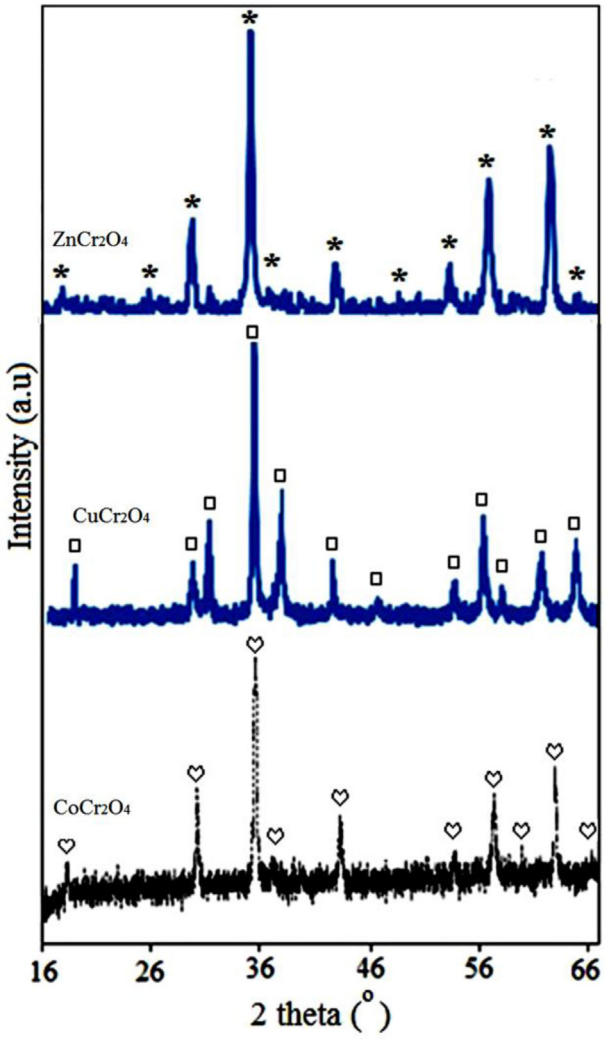

Fig. 1. X-ray diffraction patterns of MCr_2O_4 (M=Cu, Co, and Zn) catalysts. Top: $ZnCr_2O_4$; middle: $CuCr_2O_4$, and bottom: $CoCr_2O_4$.

In order to confirm the spinel structure of the catalysts, FTIR analysis was carried out (spectra not shown here). As stated in literature [23,28], the spinel-type oxides show two bands in the 700–400 cm^{-1} region corresponding to the stretching vibration of metal oxygen bond. The band around 500 cm^{-1} is assigned to the vibration of metal atom (A) in the tetrahedral environment of oxygen atom (A–O) and the band above 600 cm^{-1} corresponds to the vibration of metal atom (B) in the octahedral (Oh) site of spinel. Appearance of these bands confirmed the formation of spinel structures. The bands around 615, 611, and 621 cm^{-1} correspond to bending modes of vibration of Cr–O in the Oh sites of spinels and those around 496, 507, and 503 cm^{-1} correspond to bending modes of vibration of Co–O, Cu–O and Zn–O in $CoCr_2O_4$, $CuCr_2O_4$ and $ZnCr_2O_4$, respectively. The difference in the position of the bands in the IR spectra of samples is due to the mutual interaction of metal ions (A and B) occurring in tetrahedral and octahedral sub-lattices respectively. The broad band in the region around 3400 cm^{-1} is attributed to the presence of coordinated water and bands around 1560 cm^{-1} are ascribed to the presence of trace organic compounds [29].

The results of specific surface area, pore size, and pore volume measurements of samples are presented in Table 2. Among the different samples, $CoCr_2O_4$ shows the highest surface area value (24.1 cm^2/g), whereas $CuCr_2O_4$ shows the lowest. The following order for the specific surface area, pore size and pore volume of samples is found: $CoCr_2O_4 > ZnCr_2O_4 > CuCr_2O_4$.

The morphology of spinel catalysts was investigated by scanning electron microscopy. The SEM images are shown in Fig. 2. All the samples displayed similar morphology and

Table 2
BET specific surface area and pore properties of samples.

Sample	BET surface area (cm^2/g)	Pore volume (cm^3/g)	Pore size (Å)
$CuCr_2O_4$	8.5	0.023	54.4
$CoCr_2O_4$	24.1	0.148	123.1
$ZnCr_2O_4$	11.9	0.030	55.1

Table 1
Structural properties of MCr_2O_4 spinel catalysts.

Sample	Crystal system	Cell constants			Space group	Cell volume (Å^3)	Crystallite average size (nm)
		a	*b*	*c*			
$CuCr_2O_4$	Tetragonal	6.033	6.033	7.782	I42d	284.0	40
$CoCr_2O_4$	Cubic	8.328	8.328	8.328	Fd3m	578.0	40
$ZnCr_2O_4$	Cubic	8.328	8.328	8.328	Fd3m	577.4	37

particle sizes however it appears that $CoCr_2O_4$ is less uniform than $CuCr_2O_4$ and $ZnCr_2O_4$. Their surfaces consist of sphere-like grains that are agglomerated and exhibit largely open porous structure. The mean size of spinel particles in the mixed oxides ranges from 40 to 80 nm being closer to 80 nm in the case of the Cu chromite spinel. The comparison between the

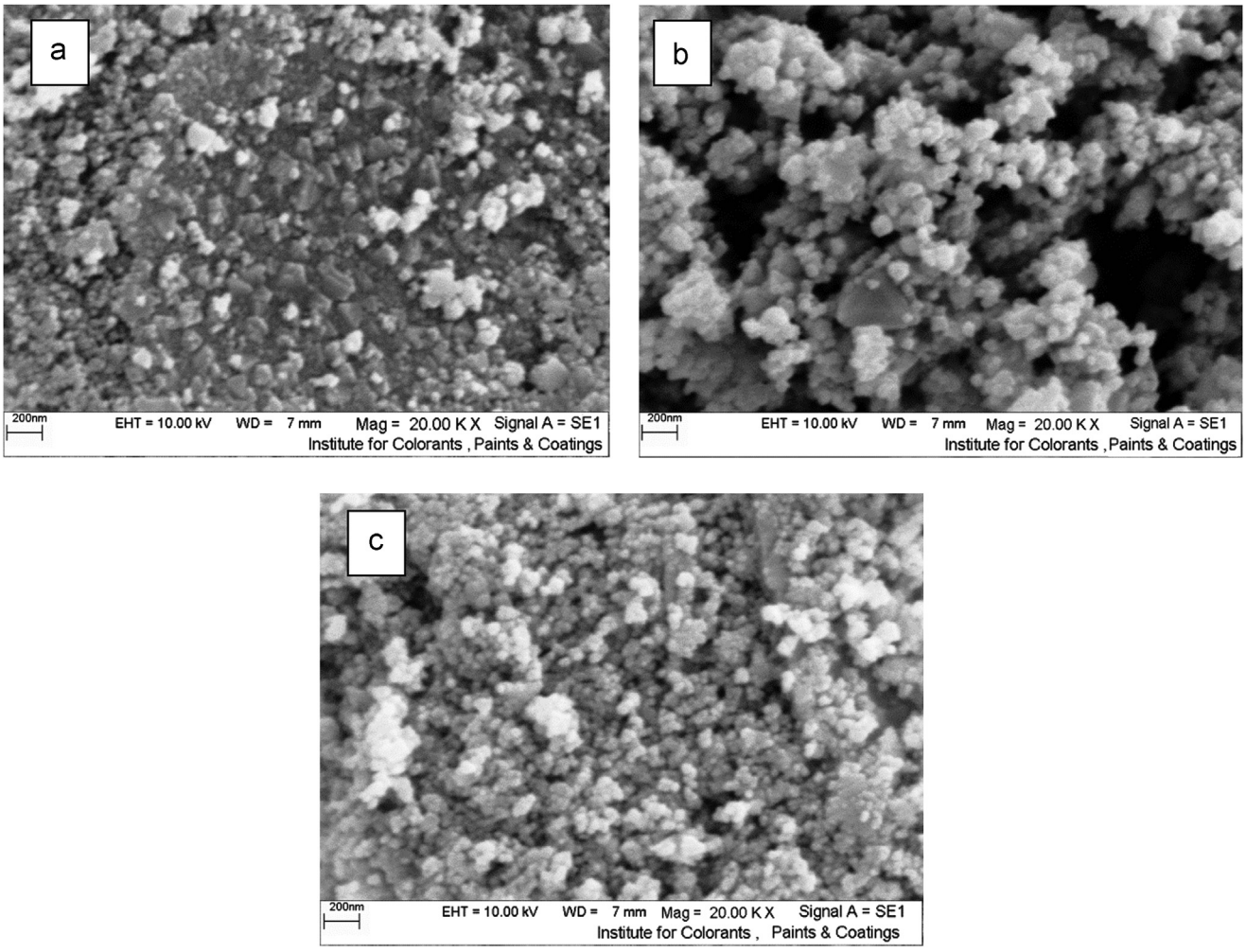

Fig. 2. Scanning electron microscopy images of $CoCr_2O_4$ (a), $CuCr_2O_4$ (b), and $ZnCr_2O_4$ (c).

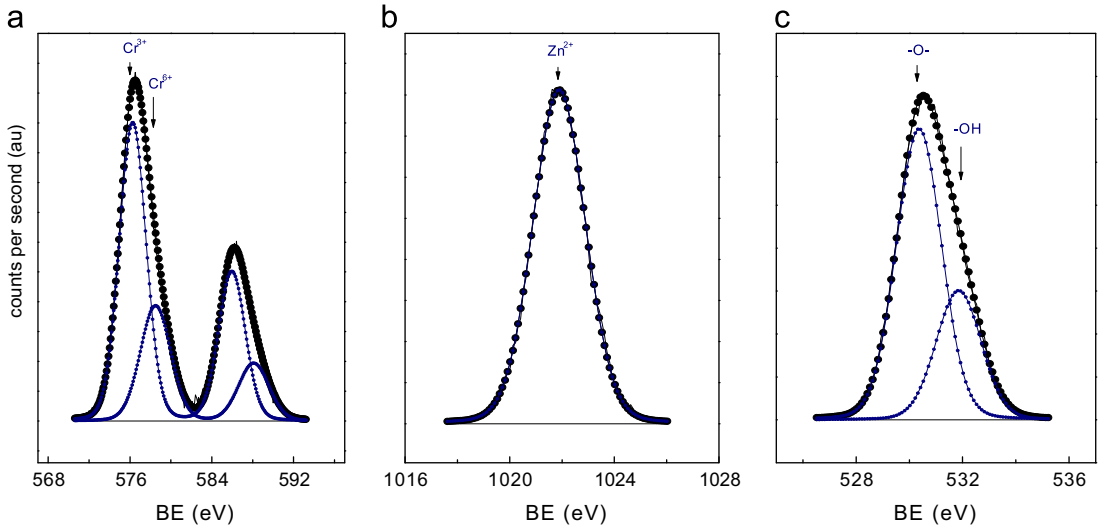

Fig. 3. XP spectra of $ZnCr_2O_4$ spinel: (a) Cr 2p core-level spectrum; (b) Zn $2p_{3/2}$ core-level spectrum; and (c) O 1s core-level spectrum.

average particle size, from SEM results, and the mean crystallite size or grain from XRD, indicate that each particle is constituted by one to two crystallites.

The chemical state and surface compositions of the fresh MCr_2O_4 (M=Zn, Cu, and Co) catalyst were determined by XPS. The Cr 2p, Zn $2p_{3/2}$ and O1s core-level spectra of the fresh $ZnCr_2O_4$ catalyst are depicted in Fig. 3a–c. The binding energies of the elements are listed in Table 3. Two chromium species were found of the Cr 2p peaks: the most intense Cr $2p_{3/2}$ peak revealed the presence of two chromium species at 576.3 eV (Cr^{3+}) and 578.5 eV (Cr^{6+}), which are similar to that reported for chromite species [30]. The percentage of the high and low valence chromium species on the catalyst surface was 30% and 70%, respectively. The binding energy of the Zn $2p_{3/2}$ core-level in this catalyst is 1021.8 eV indicating that most of the Zn is present as spinel species [31]. In addition, the O1s peak exhibited two components: a major one at 530.4 eV (69% of total area) and a minor one at 531.7 eV (31% of total area), usually assigned to lattice oxygen and surface hydroxyl groups, respectively [32]. Quantitative XPS measurements also showed that the atomic surface ratio Zn/Cr is 0.456 (Table 3) which is close to the stoichiometric value (Zn/Cr=0.500 in $ZnCr_2O_4$).

Table 3
Binding energies (eV) of core-levels and M/Cr surface ratios of MCr_2O_4 catalysts.

Catalyst	Cr $2p_{3/2}$	M $2p_{3/2}$	O1s	M/Cr at
$ZnCr_2O_4$	576.3 (70)		530.4 (69)	
	578.5 (30)	Zn $2p_{3/2}$=1021.8	531.7 (31)	0.456
$CuCr_2O_4$	576.3 (65)	Cu $2p_{3/2}$=934.8 (93)	529.9 (57)	
	578.8 (35)	Cu $2p_{3/2}$=932.2 (7)	531.4 (43)	0.511
$CoCr_2O_4$	576.3 (76)		530.5 (74)	
	578.6 (24)	Co 2p3/2=780.9	531.5 (26)	0.493

In parentheses are peak percentages.

Similarly, the Cr 2p, Cu 2p and O1s core-level spectra of the $CuCr_2O_4$ spinel are displayed in Fig. 4a–c and the corresponding binding energies of the elements are also listed in Table 3. The Cr $2p_{3/2}$ spectrum of $CuCr_2O_4$ catalyst shows also two chromium species at 576.3 eV (Cr^{3+}, 65% contribution) and 578.8 eV (Cr^{6+}, 35% contribution). The Cu $2p_{3/2}$ profile of this catalyst presents a major component at 934.8 eV, which is characteristic of Cu^{2+} ions in spinel like structures [33]. This assignment is also consistent with the observation of strong satellite line (see Fig. 4b) observed in the high binding energy side of the principal line. A minor component (7% of total area) at 932.2 eV, originated from Cu^{+} ions stabilized in the spinel lattice was also observed. The atomic ratio Cu/Cr=0.511 (Table 3) for this catalyst is very close to the stoichiometric ratio (Cu/Cr=0.500).

Finally, the Cr 2p, Co 2p and O1s core-level spectra of the $CoCr_2O_4$ sample are shown in Fig. 5a–c and the respective binding energies of the elements are also collected in Table 3. As for the Zn- and Cu-chromites, the Cr $2p_{3/2}$ spectrum of $CoCr_2O_4$ catalyst shows also two chromium components at 576.3 eV (Cr^{3+}, 76% contribution) and 578.6 eV (Cr^{6+}, 24% contribution). The most intense Co $2p_{3/2}$ peak of the Co 2p doublet at a binding energy of 780.9 eV and observation of a broad satellite line placed in the high binding energy side of the principal peak are consistent with the presence of Co^{2+} ions in a $CoCr_2O_4$ spinel structure [34]. Some Co_3O_4 surface phase cannot be discarded either. There is close similarity of the surface Co/Cr ratio (0.493) and the theoretical one of pure $CoCr_2O_4$ (0.500).

The reducibility of the MCr_2O_4 catalysts was investigated by temperature-programmed reduction. The H_2-consumption profiles of $CoCr_2O_4$, $CuCr_2O_4$, and $ZnCr_2O_4$ are shown in Fig. 6. From these profiles it is evident that the nature of element M has a great influence on the reduction profiles. The reduction profile of $CuCr_2O_4$ catalyst shows different peaks. In accordance with previous results reported in literature for a

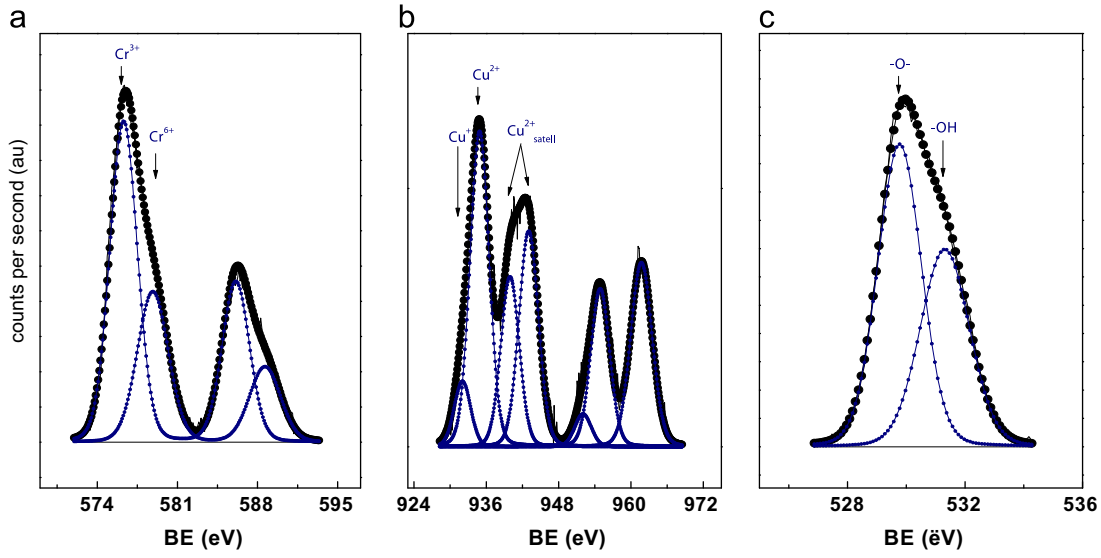

Fig. 4. XP spectra of $CuCr_2O_4$ spinel: (a) Cr 2p core-level spectrum; (b) Cu 2p core-level spectrum; and (c) O 1s core-level spectrum.

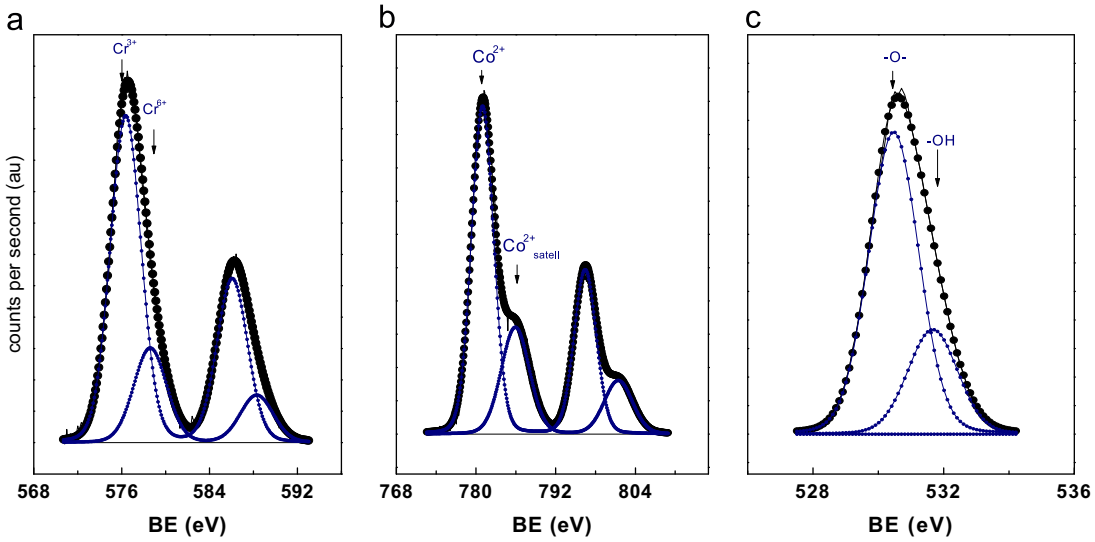

Fig. 5. XP spectra of $CoCr_2O_4$ spinel: (a) Cr 2p core-level spectrum; (b) Co 2p core-level spectrum; and (c) O 1s core-level spectrum.

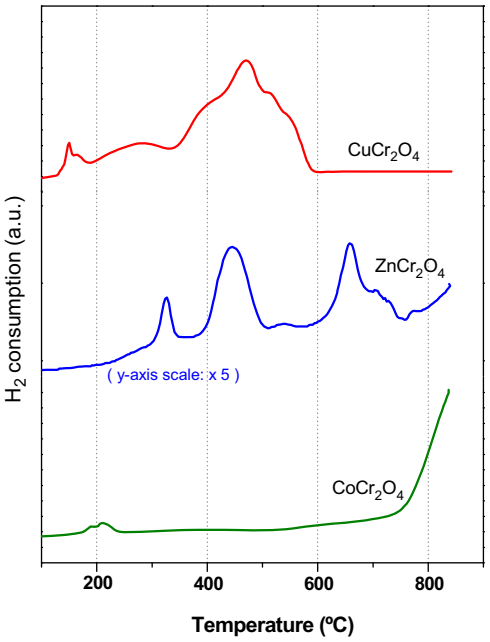

Fig. 6. Temperature-programmed reduction (TPR) profiles of catalysts. Catalysts are labeled inside figure.

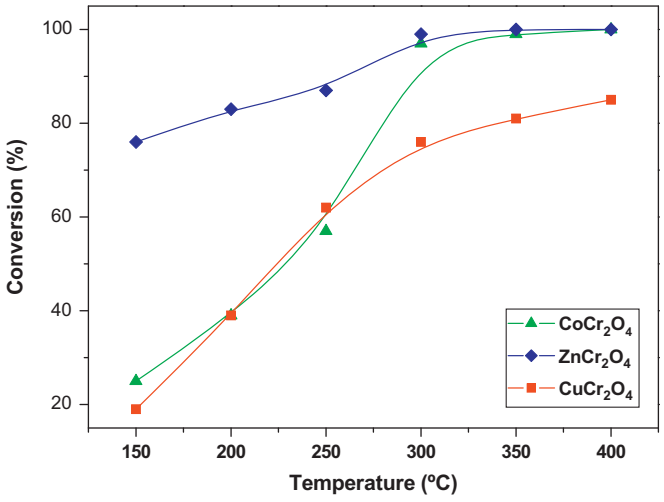

Fig. 7. Light-off curves for combustion of 2-propanol on $CoCr_2O_4$, $CuCr_2O_4$ and $ZnCr_2O_4$. Reaction conditions were: 0.20 g catalyst and 2-propanol/N_2=0.2 vol%.

similar system, the first reduction peak centered around 160 °C which could be attributed to the reduction of small and highly dispersed CuO particles [35], and a second peak at 270 °C originated from the reduction of surface CrO_3 particles. Indeed, it is often reported in bibliography that a fraction of the exposed Cr^{3+} ions in chromium oxide becomes readily oxidized to Cr^{6+} along the calcination step in ambient atmosphere (see XPS analysis above) [36]. Above 400 °C, there is a main reduction consumption which is attributed to the reduction of bulk Cu^{2+} ions of $CuCr_2O_4$ to $CuCrO_2$, and to the mixed oxide toward Cu^0 and Cr_2O_3 [35,37].

The reduction profile of $CoCr_2O_4$ also shows a H_2-consumption peak at low temperatures (≈200–230 °C) which, in agreement with the above, is also attributed to the reduction of Co_3O_4 and CrO_3 phases present on the surface of $CoCr_2O_4$ spinel (see Fig. 5a and b). The H_2-consumption around 550–750 °C could include the chemisorption of hydrogen whereas the last H_2-consumption starting at temperature somewhere about 750 °C comes from the reduction of Co^{2+} ions present in the $CoCr_2O_4$ lattice into Co^0 and Cr_2O_3 [38].

Finally the reduction profile of $ZnCr_2O_4$ catalyst, characterized by a weak reduction consumption, exhibits a small H_2-consumption peak around 225 °C is assigned to the reduction of surface CrO_3 phase present on the surface of $ZnCr_2O_4$ particles [36]. The peak around 440 °C is related to the reduction of Cr^{6+} in another surface phase such as $ZnCrO_4$ to Cr^{3+} or even to activate hydrogen adsorption [39–41]. The peak around 660 °C could be attributed to the reduction of some existing ZnO particles, not incorporated to the spinel

lattice during the synthesis [42,43]. Since $ZnCr_2O_4$ is thermodynamically very stable, no reduction peaks of this phase are expected.

3.2. Catalyst performance

To evaluate the catalytic performance of synthesized spinels, 2-propanol combustion was selected as the target reaction. Activity of the catalysts is expressed as conversion of 2-propanol as a function of the reaction time. Fig. 7 depicts the results of activity tests of the three MCr_2O_4 catalysts within the temperature range 150–400 °C. It is observed that the catalytic activity of $ZnCr_2O_4$ for the conversion of 2-propanol is much higher than that shown by $CuCr_2O_4$ and $CoCr_2O_4$ counterparts. Thus, complete conversion of 2-propanol over $ZnCr_2O_4$ resulted at 250 °C, while complete conversion of 2-propanol on $CoCr_2O_4$ occurred at 300 °C. Even less active is $CuCr_2O_4$ catalyst for which a 2-propanol conversion of 84% was attained at 400 °C. In all cases, at temperatures above 300 °C most of the products were carbon dioxide and water (> 90%), and acetone, acetaldehyde, and carbon monoxide were less than ten percent under the selected reaction conditions employed in this work.

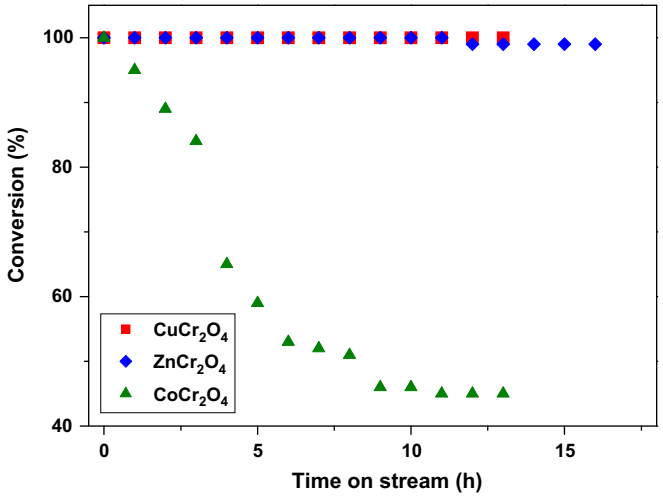

Fig. 8. Conversion vs. time on-stream curves for 2-propanol combustion on different spinel catalysts. Labeling is included inside figure.

The results of this work, together with our previous findings [23], pointed out that among the various spinel oxides such as chromites, manganites and cobaltites, with different elements in the M position of the spinel, the $ZnCr_2O_4$ exhibited the highest activity for combustion of volatile organic compounds [23]. In addition, these mixed oxide catalysts showed higher activities than single oxide catalysts [3,21]. As observed in Fig. 7, it should be noted that the activity and reducibility of the catalysts for this oxidation reaction follow an opposite trend.

In addition to the activity tests, some additional experiments were conducted to examine the stability of catalysts in the combustion of 2-propanol at a reaction temperature of 280 °C. The profiles of 2-propanol conversion for periods on-stream of 13 h are displayed in Fig. 8. From the data collected in Fig. 8 it is clear that the conversion of 2-propanol over $ZnCr_2O_4$ and $CuCr_2O_4$ catalysts reached ca. 98% whereas in the case of $CoCr_2O_4$ activity dropped to ca. 47% after 13 h on-stream.

3.3. Activity-structure correlation

For metal oxide catalysts, the reduction of surface sites at the reaction temperatures is the main reason for activity drop. In order to study the correlation between surface properties and stability of catalysts and to reveal accordingly the nature of active sites for the total oxidation of 2-propanol, surface analyses of the used catalyst was conducted by photoelectron spectroscopy.

Fig. 9 depicts the Cr 2p spectra of the three used catalysts and Table 4 summarizes the corresponding binding energies of Cr $2p_{3/2}$, Zn $2p_{3/2}$, Cu $2p_{3/2}$ and Co $2p_{3/2}$ core levels together with the surface M/Cr (M=Zn, Cu, and Co) atomic ratio.

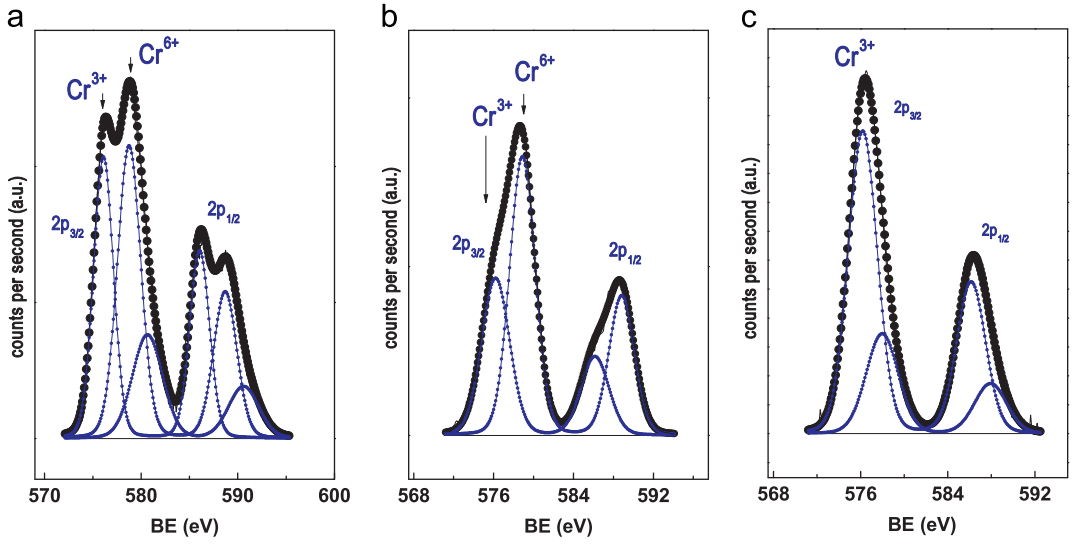

Fig. 9. Cr 2p core-level spectra of used $CuCr_2O_4$ (a), $ZnCr_2O_4$ (b), and $CoCr_2O_4$ (c) catalysts in stability tests.

Table 4
Binding energies (eV) of core-levels and M/Cr surface ratios of used catalysts.

Catalyst	Cr $2p_{3/2}$	M $2p_{3/2}$	M/Cr at
$ZnCr_2O_4$	576.5 (38) 578.8 (63)	Zn $2p_{3/2}$=1021.6	0.193
$CuCr_2O_4$	576.3 (65) 578.8 (35)	Cu $2p_{3/2}$=935.0	0.508
$CoCr_2O_4$	576.2 (100)	Co $2p_{3/2}$=781.0	0.428

In parentheses are peak percentages.

As for the fresh MCr_2O_4 catalysts, the Cr 2p emission was satisfactorily fitted to two components; the most intense Cr $2p_{3/2}$ shows contributions at 576.1–576.5 and 578.8 eV corresponding, as stated above, to Cr^{3+} and Cr^{6+}, respectively (Fig. 9). The Cr^{6+}/Cr_{total} ratio followed the order: 63% for $ZnCr_2O_4$ and 35% for $CuCr_2O_4$ spinel. In the case of $CoCr_2O_4$, just Cr^{3+} ion component was only observed. For this later catalyst, in spite of having the largest surface area, the lowest performance was recorded. Thus, according to the Mars van Krevelen mechanism, that involves reaction of VOC molecule and oxygen on redox site, the higher activity and stability of $ZnCr_2O_4$ and $CuCr_2O_4$ for total oxidation of 2-propanol is ascribed to presence of a higher amount of surface oxygen related to a higher proportion of Cr^{6+} species at the surface of these catalysts. On the basis of TPR data, it is emphasized that oxygen once activated at Cr^{6+}–O–Cr^{6+} sites is released at temperatures within the range of that at which catalytic combustion of 2-propanol occurs.

Finally, although the ratio M/Cr is the lowest for the used $ZnCr_2O_4$ spinel (Table 4), this parameter does not appear to have a major role in the catalytic performance of these spinels. On the contrary, the capability of the MCr_2O_4 catalyst to stabilize Cr^{6+} ions at the catalyst surface during the reaction is the key parameter controlling reactivity. This result is in agreement with those reported by other authors [10,13,38], who found a higher capability to deliver surface, weakly chemisorbed oxygen species at Cr^{6+}–O–Cr^{6+} sites.

4. Conclusions

In summary, three chromite spinels were successfully synthesized by the sol–gel combustion method and the relationship between their structure and catalytic properties was investigated. Preliminary catalytic data reveal that $ZnCr_2O_4$ exhibited the highest activity toward 2-propanol combustion. It is concluded that the activity and stability of studied chromites for the oxidation of 2-propanol depended on surface oxygen availability, related to stabilization of a higher proportion of Cr^{6+} sites. The high stability $ZnCr_2O_4$ and $CuCr_2O_4$ is attributed to their ability to stabilize weakly bonded oxygen at Cr^{6+}–O–Cr^{6+} sites under the reaction conditions selected in this work. Nano spinel chromites, especially $ZnCr_2O_4$ spinel, with a greater proportion of surface oxygen, could be promising as catalyst in the catalytic combustion of volatile organic compounds.

Acknowledgments

This project was financially supported by Iranian Nanotechnology Initiative Council.

References

[1] W.J. Ma, Q. Huang, Y. Xu, Y.W. Chen, S.M. Zhu, S.B. Shen, Catalytic combustion of toluene over Fe–Mn mixed oxides supported on cordierite, Ceramics International 39 (2013) 277–281.
[2] L.F. Liotta, Catalytic oxidation of volatile organic compounds on supported noble metals, Applied Catalysis B 100 (2010) 403–412.
[3] S.A. Hosseini, A. Niaei, D. Salari, S.R. Nabavi, Nanocrystalline AMn_2O_4 (A=Co, Ni, and Cu) spinels for remediation of volatile organic compounds-synthesis, characterization and catalytic performance, Ceramics International 38 (2012) 1655–1661.
[4] C. Lahousse, A. Bernier, B. Delmon, P. Papaefthimiou, T. Ionnides, X.E. Verykios, Evaluation of γ-MnO_2 as a VOC removal catalyst: comparison with a noble metal catalyst, Journal of Catalysis 178 (1998) 214–225.
[5] R. Insley, US Patent US3995184, 1985.
[6] C.L. Adridge, US Patent US04456703, 1984.
[7] S.C. Kim, The catalytic oxidation of aromatic hydrocarbons over supported metal oxide, Journal of Hazardous Materials 91 (2002) 285–299.
[8] J. Kirchnerova, D. Klvana, Design criteria for high-temperature combustion catalysts, Catalysis Letters 67 (2000) 175–181.
[9] P. Stefanov, I. Avramova, D. Stoichev, N. Radic, B. Grbic, T. Marinova, Characterization and catalytic activity of Cu–Co spinel thin films catalysts, Applied Surface Science 245 (2005) 65–72.
[10] D. Kim, S. Ihm, Application of spinel-type cobalt chromiteas a novel catalyst for combustion of chlorinated organic pollutants, Environmental Science and Technology 35 (2001) 222–226.
[11] U. Zavyalova, V.F. Tretyakov, T.N. Burdeynaya, V.V. Lunin, A.I. Titkov, A.N. Salanov, P.G Tsyrulnikov, Petroleum Chemistry 45 (2005) 255–264.
[12] D. Fino, N. Russo, G. Saracco, V. Specchia, Catalytic removal of NO_x and diesel soot over nanostructured spinel-type oxides, Journal of Catalysis 242 (2006) 38–47.
[13] H.G. El-Shobaky, Surface and catalytic properties of Co, Ni and Cu binary oxide systems, Applied Catalysis A 278 (2004) 1–9.
[14] L. Yan, T. Ren, X. Wang, Q. Gao, D. Ji, J. Suo, Excellent catalytic performance of $Zn_xCo_{1-x}Co_2O_4$ spinel catalysts for the decomposition of nitrous oxide, Catalysis Communications 4 (2003) 505–509.
[15] Z. Ma, Z. Xiao, J. Bokhoven, C. Liang, A non-alkoxide sol–gel route to highly active and selective Cu–Cr catalysts for glycerol conversion, Journal of Materials Chemistry 20 (2010) 755–760.
[16] R.M. Gabr, M.M. Girgis, A.M. El-Award, Formation, conductivity and activity of zinc chromite catalyst, Materials Chemistry and Physics 30 (1992) 169–177.
[17] M. Qian, H.C. Zeng, Synthesis and characterization of Mg–Co catalytic oxide materials for low-temperature N_2O decomposition, Journal of Materials Chemistry 7 (1997) 493–499.
[18] L. Markov, A. Lyubchova, Precursor control of the inversion degree of magnesium–cobalt spinels, Materials Science Letters 10 (1991) 512–514.
[19] L. Castro, P. Reyes, C. Montes, Synthesis and characterization of sol–gel Cu–ZrO_2 and Fe–ZrO_2 catalysts, Journal of Sol–Gel Science and Technology 25 (2002) 159–168.
[20] Y. Fan, X. Lu, Y. Ni, H. Zhang, L. Zhao, J. Chen, C. Sun, Destruction of polychlorinated aromatic compounds by spinel-type complex oxides, Environmental Science and Technology 44 (2010) 3079–3084.
[21] A. Niaei, D. Salari, F. Aghazadeh, N Çaylak, A. Sepehrianazar, Catalytic oxidation of 2-propanol over (Cr,Mn,Fe)-Pt/γ-Al_2O_3 bimetallic catalysts and modeling of experimental results by artificial neural networks, Journal of Environmental Science and Health, Part A 45 (2010) 454–463.
[22] S.A. Hosseini, M. Sadeghi, A. Alemi, A. Niaei, D. Salari, L. Kafi, Synthesis, characterization, and performance of $LaZn_xFe_{1-x}O_3$ perovskite

nanocatalysts for toluene combustion, Chinese Journal of Catalysis 31 (2010) 747–750.
[23] S.A. Hosseini, D. Salari, A. Niaei, F. Deganello, G. Pantaleo, P. Hojatti, Chemical–physical properties of spinel $CoMn_2O_4$ nano-powders and catalytic activity in the 2-propanol and toluene combustion: effect of the preparation method, Journal of Environmental Science and Health, Part A 46 (2011) 291–297.
[24] L.B. Mc Cusker, R.B. Von Dreele, D.E. Coxd, D. Louer, P. Scardi, Rietveld refinement guidelines, Applied Crystallography 32 (1999) 36–50.
[25] National Bureau of Standard Monograph 25, Section 9, 1971, pp. 59.
[26] National Bureau of Standard Monograph 25, Section 20, 1983, pp. 46.
[27] P.N. Satish, B. Basavalingu, J.A.K. Tareen, Unusual twinning in spinel ($CoCr_2O_4$) phase, Journal of Crystal Growth 54 (1981) 592–594.
[28] A.V. Salker, S.M. Gurav, Electronic and catalytic studies on $Co_{1-x}Cu_xMn_2O_4$ for CO oxidation, Journal of Materials Science 35 (2000) 4713–4719.
[29] U. Zavyalova, B. Nigrovski, K. Pollok, F. Langenhorst, B. Müller, P. Scholz, B. Ondruschka, Gel-combustion synthesis of nanocrystalline spinel catalysts for VOCs elimination, Applied Catalysis B 83 (2008) 221–228.
[30] T. Mega, K. Takao, J. Shimomura, State analysis of electrolytic chromate film by XPS and SXS, Applied Surface Science 121–122 (1997) 120–124.
[31] Y. Zhang, W. Xu, J. Zhao, Synthesis of phenylacetonitrile by amination of styrene oxide catalyzed by a bimetallic catalyst $Zn_{30.1}Cr_{4.3}/\gamma$-Al_2O_3, RSC Advances 2 (2012) 6590–6598.
[32] J.L.G. Fierro, Metal Oxides: Chemistry and Applications, Taylor and Francis, Florida, 2000.
[33] R.T. Figueiredo, M. Lopez-Granados, A. Martinez-Arias, J.L.G. Fierro, Spectroscopic evidence of Cu–Al interactions in Cu–Zn–Al mixed oxide catalysts used in CO hydrogenation, Journal of Catalysis 178 (1) (1998) 146–152.
[34] N. Ballarini, F. Cavani, S. Passeri, L. Pesaresi, A.F. Lee, K. Wilson, Phenol methylation over nanoparticulate $CoFe_2O_4$ inverse spinel catalysts: the effect of morphology on catalytic performance, Applied Catalysis A 366 (2009) 184–192.
[35] K.L. Deutsch, B.H. Shanks, Active species of copper chromite catalyst in C–O hydrogenolysis of 5-methylfurfuryl alcohol, Journal of Catalysis 285 (2012) 235–241.
[36] B. Grzybowska, J. Sloczynski, R. Grabowski, K. Wcislo, A. Kozlowska, J. Stoch, J. Zielinski, Chromium oxide/alumina catalysts in oxidative dehydrogenation of isobutane, Journal of Catalysis 178 (1998) 687–700.
[37] A. Iimura, Y. Inoue, I. Yasumori, The effect of hydrogen reduction on the composition, structure, and catalytic activity of methanol decomposition, Bulletin of the Chemical Society of Japan 56 (1983) 2203–2207.
[38] Y. Wang, P. Yang, G. Liu, L. Xu, M. Jia, W. Zhang, D. Jiang, Stability and deactivation of spinel-type cobalt chromite catalysts for ortho-selective alkylation of phenol with methanol, Catalysis Communications 9 (2008) 2044–2047.
[39] F. Simard, U.A. Sedran, J. Sepúlveda, N.S. Fígoli, H.I. de Lasa, $ZnOCr_2O_3$+ZSM-5 catalyst with very low Zn/Cr ratio for the transformation of synthesis gas to hydrocarbons, Applied Catalysis A 125 (1995) 81–98.
[40] M.F.M Zwinkels, O. Haussner, P. Govind Menon, S.G. Järås, Preparation and characterization of $LaCrO_3$ and Cr_2O_3 methane combustion catalysts supported on $LaAl_{11}O_{18}$- and Al_2O_3-coated monoliths, Catalysis Today 47 (1999) 73–82.
[41] M. Wojciechowska, I. Tomska-Foralewska, W. Przystajko, M. Zieliński, Catalytic properties of Cr_2O_3 doped with MgO supported on MgF_2 and Al_2O_3, Catalysis Letters 104 (2005) 121–128.
[42] A. Venugopal, R. Sarkari, C. Anjaneyulu, V. Krishna, M.K. Kumar, Cu–Zn–Cr_2O_3 catalysts for dimethyl ether synthesis: structure and activity relationship, Catalysis Letters 123 (2008) 142–149.
[43] R. Kam, C. Selomulya, R. Amal, J. Scott, The influence of La-doping on the activity and stability of Cu/ZnO catalyst for the low-temperature water–gas shift reaction, Journal of Catalysis 273 (2010) 73–81.